J Mater Sci (2009) 44:919–925
DOI 10.1007/s10853-008-3190-0

Coprecipitation synthesis and optical absorption property of $Zn_2Ti_xSn_{1-x}O_4$ ($0 \leq x \leq 1$) solid solutions

Cun Wang · Bo-Qing Xu

Received: 4 May 2008 / Accepted: 12 December 2008 / Published online: 31 December 2008

Abstract We report a coprecipitation method for the preparation of solid solutions in the $Zn_2Ti_xSn_{1-x}O_4$ ($0 \leq x \leq 1$) series. The precipitates obtained from the coprecipitation were calcined using different temperatures and then characterized with X-ray diffraction (XRD), Raman scattering (RS), scanning electron microscopy (SEM), and surface area measurements to gain insights into the solid-state reaction and phase transformation during the calcinations. Formation of the $Zn_2Ti_xSn_{1-x}O_4$ solid solutions was observed after the calcination up to 1000 °C, which is much lower than the temperature (1300 °C) required in the conventional solid-state reaction method. The optical absorption property of the $Zn_2Ti_xSn_{1-x}O_4$ solid solutions, measured by ultraviolet-visible diffuse reflectance spectroscopy (UV–Vis DRS), was shown to change according to the composition of the solid solutions.

Introduction

In the past several decades, special attentions have been paid to the systems of many binary oxides such as TiO_2–SnO_2 [1–5], ZnO–TiO_2 [6–10], and ZnO–SnO_2 [11–14] due to their expected wide range of applications.

C. Wang (✉) · B.-Q. Xu (✉)
Key Lab of Organic Optoelectronics & Molecular Engineering, Tsinghua University, 100084 Beijing, China
e-mail: wangcun988@126.com

B.-Q. Xu
e-mail: bqxu@mail.tsinghua.edu.cn

TiO_2 and SnO_2 in the TiO_2–SnO_2 system can exist in $Ti_xSn_{1-x}O_2$ ($0 \leq x \leq 1$) solid solutions with a rutile structure [1, 4, 15–18]. The TiO_2–SnO_2 system has found some applications as photocatalysts [3, 17] and gas-sensing materials [2, 15, 18]. The ZnO–TiO_2 system can be obtained in three different crystal phases: $ZnTiO_3$ (hexagonal), $Zn_2Ti_3O_8$ (cubic), and Zn_2TiO_4 (cubic) [6–9, 19, 20], depending on the composition and preparation conditions [6–9, 19, 20]. Both $ZnTiO_3$ and Zn_2TiO_4 phases could find applications as microwave dielectric and catalytic materials [21–23]. On the other hand, the ZnO–SnO_2 system can be obtained as stable $ZnSnO_3$ (cubic) or Zn_2SnO_4 (cubic) phase, according to composition and method of preparation including the final calcination temperature [24–27]. The $ZnSnO_3$ phase could have interesting optical, electrical, and gas-sensing properties, which may find applications in optoelectrical [28], gas-sensing [26, 29] and lithium ion battery materials [30]. The Zn_2SnO_4 phase could also show similar properties and potential of applications [31–33].

In our previous works [34, 35], polycrystalline $Zn_2Ti_xSn_{1-x}O_4$ ($0 \leq x \leq 1$) solid solutions were prepared at 1300 °C with a solid-state reaction method. The as-prepared $Zn_2Ti_xSn_{1-x}O_4$ ($0 \leq x \leq 1$) solid solutions were found to exhibit ultraviolet-visible optical absorption property according to the content of titanium. In the present work, we report a coprecipitation method for the preparation of polycrystalline $Zn_2Ti_xSn_{1-x}O_4$ ($0 \leq x \leq 1$) materials, which leads to a temperature lowering to about 1000 °C for the formation of the solid solutions. The solid solution products are characterized with X-ray diffraction (XRD), Raman scattering (RS), scanning electron microscopy (SEM), and specific surface area measurements. Ultraviolet-visible diffuse reflectance spectroscopy (UV–Vis DRS) study of the as-prepared $Zn_2Ti_xSn_{1-x}O_4$ ($0 \leq x \leq 1$) solid solutions is also reported.

Experimental

Coprecipitation synthesis of materials

All of the chemical reagents used in this work were of analytic reagent grade (A.R.) and were purchased from the Beijing Shuanghuan Chemicals Factory, China. $ZnCl_2$, $Ti(SO_4)_2$ and $SnCl_4$ $5H_2O$ were used as the starting metal salts, and NaOH as the precipitant in the coprecipitation preparation of $Zn_2Ti_xSn_{1-x}O_4$ ($x = 0$, 0.1, 0.3, 0.5, 0.7, 0.9, 1.0) materials. Detailed procedure for the preparation was as follows: a solution mixture containing stoichiometric amounts of $ZnCl_2$, $Ti(SO_4)_2$ and $SnCl_4$ $5H_2O$ was made by dissolving the starting metal salts with a minimum amount of deionized water. A 4 mol/L NaOH solution was then added into the solution mixture under vigorous stirring until pH $= 7.0 \pm 0.2$, which resulted in the formation of a white coprecipitate in the solutions. The coprecipitates were separated by filtration and then washed with deionized water until no SO_4^{2-} and Cl^- ions were detected in the filtrates by $Ba(NO_3)_2$ and/or $AgNO_3$ solutions. The washed coprecipitate was then dried in static ambient air at about 100 °C to prepare a dry sample of $ZnO/TiO_2/SnO_2$ precursor. Finally, the dried precursor was calcined in static ambient air at a temperature in the range of 300–1300 °C for 2 h to induce possible solid-state reactions. The products thus obtained were then ground thoroughly in an agate mortar to prepare the powder samples.

Characterization of materials

The XRD analysis was carried out at room temperature with a Bruker D8 Advance diffractometer using Cu K_α radiation ($\lambda = 1.5406$ Å). The accelerating voltage, emission current, and scanning speed were 40 kV, 40 mA, and 6°/min, respectively. Raman spectra were obtained at room temperature with a Renishaw RM2000 microscopic confocal Raman spectrometer. A 514.5-nm argon-ion laser beam with a power of 4.7 mW was used. The Raman scattering spectra were obtained with 10 scans at a resolution of 1 cm^{-1} in the range of 100–2000 cm^{-1}. SEM observations were performed with a KYKY2000 scanning electron microscope made by the Instrumental Factory of the Chinese Academy of Sciences. An operating voltage of 25 kV was used. The specific surface areas were determined based on the nitrogen adsorption data at 77 K on a Micromeritics ASAP 2010 system with the multipoint Brunauer-Emmett-Teller (BET) method [34, 35]. In order to assure the accuracy of the measured surface area data, more than 5 g sample powders were used for each measurement to ensure that each measured sample had a total surface area larger than 1.0 m^2, which is well above the detection limit of the instrument.

UV–Vis DRS

UV–Vis diffuse reflectance spectra were measured to study the optical absorption property of the samples. The spectra were recorded in air at room temperature with a Hitachi U-3010 spectrophotometer. A pure Al_2O_3 pellet (provided by Hitachi) was used as the reference sample in the measurements.

Results and discussion

XRD and crystal phase

For the sake of simplicity, the $ZnO/TiO_2/SnO_2$ mixture with a Zn/Ti/Sn molar ratio of 4:1:1 was used as a representative composition to study the solid-state reaction processes of the coprecipitated $ZnO/TiO_2/SnO_2$ mixtures. Figure 1 shows the powder X-ray diffraction patterns of the $ZnO/TiO_2/SnO_2$ mixture calcined at 300–1300 °C for 2 h. The XRD results suggest that both the phase composition and growth of the crystals were strongly related to the calcination temperature. The diffractions of the $ZnO/TiO_2/SnO_2$ mixture calcined for 2 h at 300–600 °C showed only

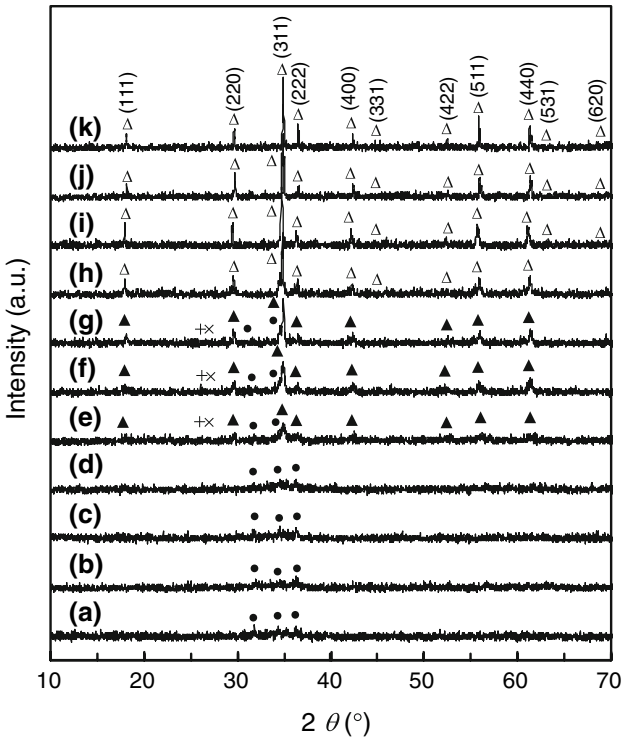

Fig. 1 XRD patterns of the $ZnO/TiO_2/SnO_2$ mixture with the $ZnO/TiO_2/SnO_2$ molar ratio of 4:1:1 prepared at 300 °C (a), 400 °C (b), 500 °C (c), 600 °C (d), 700 °C (e), 800 °C (f), 900 °C (g), 1000 °C (h), 1100 °C (i), 1200 °C (j), and 1300 °C (k), respectively, for 2 h. Crystal phases: +, anatase TiO_2; ×, cassiterite SnO_2; ●, zincite ZnO; ▲, $Zn_2Ti_xSn_{1-x}O_4$ ($0 < x < 1$); Δ, $Zn_2Ti_{0.5}Sn_{0.5}O_4$

ZnO crystals (zincite), but no crystal TiO_2 and SnO_2 phases. This indicates no formation of any new phases and the TiO_2 and SnO_2 components were still in their amorphous states, being silent to the XRD analysis after the calcination up to 600 °C. A reaction among ZnO, TiO_2, and SnO_2 to form a solid solution $Zn_2Ti_xSn_{1-x}O_4$ ($0 < x < 1$) featuring with a set of diffractions at $d = 4.8704$, 3.0314, 2.5751, 2.4702, 2.1206, 1.7447, 1.6411, and 1.5112 Å ($10° \leq 2\theta \leq 70°$), as reported in our two earlier works [34, 35], occurred after the calcination at 700 °C for 2 h. Formation of binary $ZnTiO_3$ (hexagonal) (JCPDS No. 85-0547) [7–9], Zn_2TiO_4 (cubic) (JCPDS No. 77-0014) [7–9, 34, 35] and $Zn_2Ti_3O_8$ (cubic) (JCPDS No. 73-0579) [7–9], and $ZnSnO_3$ (cubic) (JCPDS No. 28-1486) [26, 27] and Zn_2SnO_4 (cubic) (JCPDS No. 74-2184) [24, 25, 34, 35] was not detected in the XRD patterns of Fig. 1. However, small quantities of unreacted ZnO, TiO_2, and SnO_2 components still remained, in addition to $Zn_2Ti_xSn_{1-x}O_4$ ($0 < x < 1$), after the calcination at 700 °C. Therefore, compared with the solid-state reaction method [34, 35], the present coprecipitation method not only lowered the formation temperature of $Zn_2Ti_xSn_{1-x}O_4$ ($0 < x < 1$) by about 500 °C, but also enabled an one-step reaction to produce the solid solution $Zn_2Ti_xSn_{1-x}O_4$:

$$2ZnO + xTiO_2 + (1-x)SnO_2 \rightarrow Zn_2Ti_xSn_{1-x}O_4 \quad (0<x<1)$$

Thus the formation mechanism of $Zn_2Ti_xSn_{1-x}O_4$ ($0 < x < 1$) in the present coprecipitation method would be significantly different from that in the solid-state reaction method [34, 35].

After the calcinations at 800 and 900 °C, the $ZnO/TiO_2/SnO_2$ mixture was still composed of $Zn_2Ti_xSn_{1-x}O_4$ ($0 < x < 1$) and some residual oxide components (ZnO, TiO_2, and SnO_2). But the content and mean crystal size of $Zn_2Ti_xSn_{1-x}O_4$ ($0 < x < 1$) increased, while the contents of the residual oxides decreased with increasing the calcination temperature. When the calcination temperature was further raised up to 1000 °C, the whole sample became a pure solid solution phase ($Zn_2Ti_xSn_{1-x}O_4$, $0 < x < 1$) in the XRD pattern. This indicates that all of the ZnO, TiO_2, and SnO_2 components had reacted completely to form the solid solution $Zn_2Ti_xSn_{1-x}O_4$ ($0 < x < 1$). And, therefore, the product after the calcination at 1000 °C can be viewed as $Zn_2Ti_{0.5}Sn_{0.5}O_4$. This $Zn_2Ti_{0.5}Sn_{0.5}O_4$ solid solution remained as the only product in the XRD pattern when the calcination temperature was increased up to 1300 °C. However, the diffraction peaks of $Zn_2Ti_{0.5}Sn_{0.5}O_4$ were intensified gradually with the calcination temperature in the range of 1000–1300 °C, indicating that the sizes of $Zn_2Ti_{0.5}Sn_{0.5}O_4$ crystallites increased due to thermal sintering. The X-ray diffractions of $Zn_2Ti_{0.5}Sn_{0.5}O_4$ prepared at 1300 °C occurred at $d = 4.9174$, 3.0168, 2.5741, 2.4643, 2.1353, 1.9626, 1.7454, 1.6465, 1.5128, 1.4464, and 1.3534 Å ($10° \leq 2\theta \leq 70°$), featuring a face-centered cubic inverse spinel structure with a space group *Fd3m*. The pattern could be indexed exactly and the indexing results are also shown in Fig. 1. The cubic lattice constant of $Zn_2Ti_{0.5}Sn_{0.5}O_4$, calculated with the software ($Diffrac^{plus}$ Win-Metric Version 3.0) on the X-ray diffractometer, was 8.546 ± 0.003 Å. This value is larger than the lattice constant of Zn_2TiO_4 (8.4450 Å, JCPDS 77-0014) but smaller than that of Zn_2SnO_4 (8.6500 Å, JCPDS 74-2184) due to the difference in radius between Ti^{4+} (0.68 Å) and Sn^{4+} (0.71 Å). It is worth noting that the present X-ray diffraction data of $Zn_2Ti_{0.5}Sn_{0.5}O_4$ are in good agreement with those in our earlier works [34, 35].

According to the experimental results mentioned earlier, other samples of $ZnO/TiO_2/SnO_2$ mixtures prepared from the coprecipitation method were also subject to the calcinations at 1000–1300 °C for 2 h to prepare the $Zn_2Ti_xSn_{1-x}O_4$ ($0 \leq x \leq 1$) solid solutions of varying compositions (Fig. 2). It can be seen that the XRD patterns of these calcined products are very similar to each other although the regular shifts of XRD peaks toward somewhat higher angles with the increase in x in the composition of the solid solutions. All of the XRD patterns shown in Fig. 2 can be indexed successfully to the inverse spinel structure, as was observed in our two earlier works [34, 35]. The cubic lattice constants (a) of $Zn_2Ti_xSn_{1-x}O_4$ prepared at 1100 °C, calculated according to the method as mentioned previously, are 8.648, 8.634, 8.578, 8.546, 8.518, 8.480, and 8.461 Å, allowing a calculation error within ±0.003 Å, at the compositions of $x = 0$, 0.1, 0.3, 0.5, 0.7, 0.9, and 1.0, respectively. Figure 3 shows the change of lattice constant

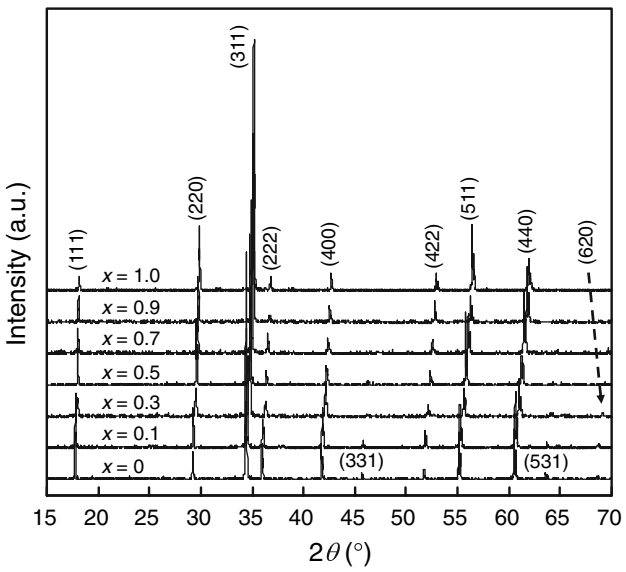

Fig. 2 XRD patterns of $Zn_2Ti_xSn_{1-x}O_4$ ($x = 0$, 0.1, 0.3, 0.5, 0.7, 0.9, 1.0) prepared at 1100 °C for 2 h

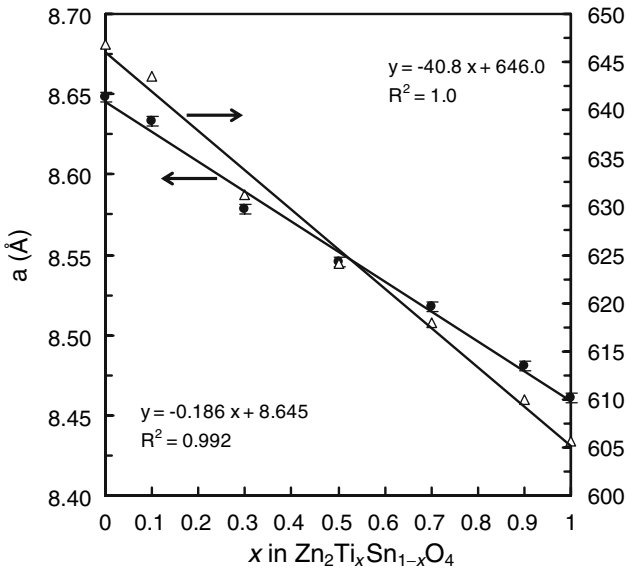

Fig. 3 Lattice parameters of $Zn_2Ti_xSn_{1-x}O_4$ ($x = 0$, 0.1, 0.3, 0.5, 0.7, 0.9, 1.0) prepared at 1100 °C for 2 h

of $Zn_2Ti_xSn_{1-x}O_4$ ($0 \leq x \leq 1$) with composition. It can be seen that the lattice constant decreases linearly with increasing x (i.e., the Ti content), obeying approximately the generally known Vegard's law. This indicates that the lattice of $Zn_2Ti_xSn_{1-x}O_4$ ($0 \leq x \leq 1$) evolves with the composition from Zn_2SnO_4 to Zn_2TiO_4, due to the substitution of lattice Ti^{4+} with a smaller radius (0.68 Å) for the Sn^{4+} with a larger radius (0.71 Å). It should be noted that the lattice constants measured in this present work of Zn_2SnO_4 ($x = 0$) and Zn_2TiO_4 ($x = 1$) are in good agreement with the standard values of 8.6500 Å for Zn_2SnO_4 (JCPDS 74-2184) and 8.4450 Å for Zn_2TiO_4 (JCPDS 77-0014). The calculated cubic unit cell volumes of $Zn_2Ti_xSn_{1-x}O_4$ ($0 \leq x \leq 1$) are 646.8, 643.6, 631.2, 624.1, 618.0, 609.8, and 605.7 $Å^3$ at the compositions of $x = 0$, 0.1, 0.3, 0.5, 0.7, 0.9, and 1.0, respectively (Fig. 3). These results agree quite well with those in our earlier works [34, 35].

Raman scattering

It is commonly accepted that inverse spinel oxides with the general formula AB_2O_4 crystallize in a cubic structure (space group O_h^7-*Fd3m*) [8, 36–42]. Although the full unit cell of the inverse spinel would contain 56 atoms ($Z = 8$) in the cubic structure, the smallest Bravais cell could only contain 14 atoms ($Z = 2$). Factor group analysis has predicted 5 Raman modes (i.e., A_{1g}, E_g and $3F_{2g}$) for the cubic spinel structure [37, 39–42].

The Raman spectra of the $Zn_2Ti_xSn_{1-x}O_4$ ($x = 0$, 0.1, 0.3, 0.5, 0.7, 0.9, 1.0) samples prepared at 1100 °C for 2 h are shown in Fig. 4a. It can be seen that the Raman spectrum of the Zn_2SnO_4 did not display all the five bands predicted by the factor group analysis of the *Fd3m* symmetry, and only 4 Raman bands were observable at 227, 377, 528, and 668 cm^{-1}. Such a difference in the number of Raman active modes between theoretical prediction and the experimental observation may be due to a poor resolution or peak overlappings [41]. But $Zn_2Ti_xSn_{1-x}O_4$ with $x = 0.3$ and 0.5 showed 7, and those with $x = 0.7$, 0.9, and 1.0 displayed 8 Raman modes. A Zn_2TiO_4 ($x = 1.0$) sample in earlier documentations [43, 44] also showed 8 Raman modes. The Raman spectrum of $Zn_2Ti_{0.1}Sn_{0.9}O_4$

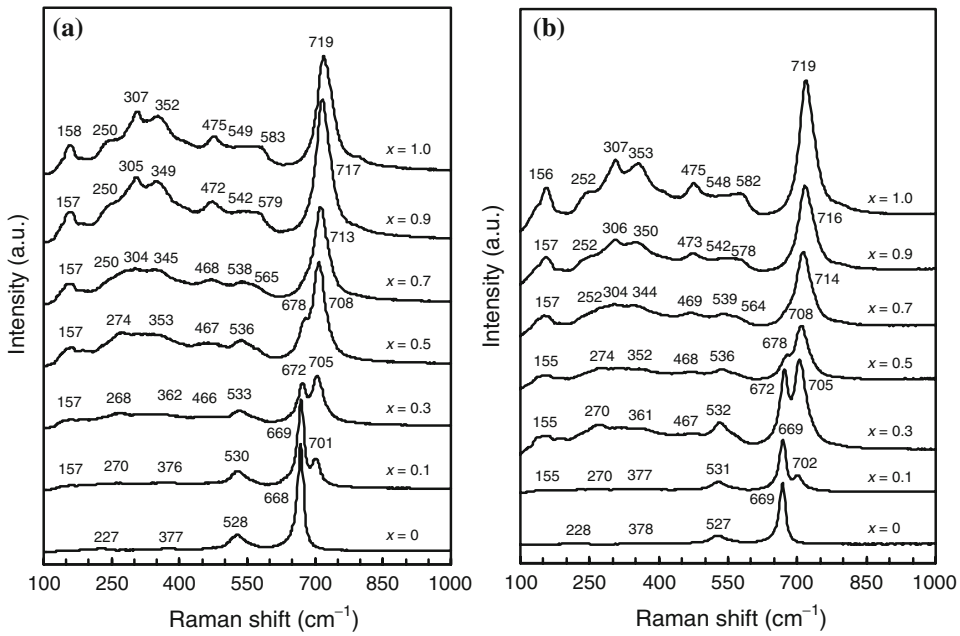

Fig. 4 Raman spectra of $Zn_2Ti_xSn_{1-x}O_4$ ($x = 0$, 0.1, 0.3, 0.5, 0.7, 0.9, 1.0) prepared at **a** 1100 °C for 2 h and **b** 1300 °C for 2 h

appeared to show all of the 5 Raman modes predicted by the factor analysis of *Fd3m* symmetry but an additional peak showed up at 701 cm^{-1} due to the incorporation of Ti^{4+} into the structure of Zn_2SnO_4. This new Raman feature was intensified and shifted toward higher wavenumbers with increasing x, while at the same time the main feature associated originally with Zn_2SnO_4 at 668 cm^{-1} was weakened and shifted also toward higher some higher wavenumbers. These changes in the Raman spectra should apparently be associated with the variation in the relative contributions of Ti–O and Sn–O bonds in the octahedral [$ZnTi_xSn_{1-x}O_6$] structure units. Since the Ti–O bond is shorter and thus stronger than the Sn–O bond, the Raman band associated with the Ti–O bond would appear at higher wavenumber than the one associated with the Sn–O bond. When the content of Ti became enough high, the intensification of the "Ti–O sensitive" Raman band would result in a disappearance of the "Sn–O sensitive" band, which explains why the "Sn–O sensitive" band became silent in the Raman spectra of the $Zn_2Ti_xSn_{1-x}O_4$ samples at $x > 0.7$. Therefore, the co-existing of the Ti–O and Sn–O sensitive Raman bands for the $Zn_2Ti_xSn_{1-x}O_4$ solid solutions at $0.1 \leq x \leq 0.7$ would imply that the Ti^{4+} and Sn^{4+} ions in these samples were not well mixed or unevenly distributed in the octahedral sites [43, 45, 46]. Moreover, the changes in "ordering" of the Ti^{4+} and Sn^{4+} ions in the octahedral sites could also be responsible for the generation of additional peaks in the range of 300–600 cm^{-1} on the Raman spectra of $Zn_2Ti_xSn_{1-x}O_4$ samples because any "ordered" structure would have a lower symmetry than the disordered parent structure [43, 45]. The disappearance of the "Sn–O sensitive" Raman mode at around 670 cm^{-1} for those $Zn_2Ti_xSn_{1-x}O_4$ samples with molar Ti/(Ti + Sn) ratio higher than 0.7 (i.e., $x > 0.7$) would suggest that Ti^{4+} and Sn^{4+} ions in these Ti-rich samples were well mixed and evenly distributed in the octahedral sites.

Figure 4b shows the Raman spectra of the $Zn_2Ti_xSn_{1-x}O_4$ ($x = 0$, 0.1, 0.3, 0.5, 0.7, 0.9, 1.0) prepared at 1300 °C. A comparison of these spectra with their counterparts in Fig. 4a would reveal that the Raman spectra of the solid solutions were little affected by increasing the calcination temperature from 1100 to 1300 °C since the spectra remained virtually unchanged in view of the errors associated with the Raman measurements (experimental resolution by wavenumber was ± 1 cm^{-1}).

SEM micrograph and BET surface area

Figure 5 shows the SEM micrographs of the $Zn_2Ti_{0.5}Sn_{0.5}O_4$ samples prepared at 1100 and 1300 °C for 2 h. The particles in the two $Zn_2Ti_{0.5}Sn_{0.5}O_4$ samples showed irregular round-like shapes, though their sizes increased remarkably when the calcination temperature was increased from 1100 (Fig. 5a) to 1300 °C (Fig. 5b).

The measured BET surface areas of the $Zn_2Ti_xSn_{1-x}O_4$ ($0 \leq x \leq 1$) samples prepared at 1100 °C for 2 h were 0.43, 0.45, 0.42, 0.41, 0.39, 0.44, and 0.43 m^2/g for $x = 0$, 0.1, 0.3, 0.5, 0.7, 0.9, and 1.0, respectively. It is not surprising that the specific surface areas of these $Zn_2Ti_xSn_{1-x}O_4$ samples were quite close to each other if one would consider the high-temperature (1100 °C) sintering they experienced during the calcinations. By assuming a spherical shape for these sintered samples, such small surface areas corresponded to a theoretical mean particle size of about 1.5 μm, which agrees basically with the morphologic feature by SEM measurement (e.g., Fig. 5a).

The surface areas were reduced to 0.23, 0.25, 0.22, 0.21, 0.24, and 0.23 m^2/g after the calcination at 1300 °C for the samples with $x = 0$, 0.1, 0.3, 0.5, 0.7, 0.9, and 1.0, respectively. These numbers correspond to a theoretical mean particle size of about 10 μm in spherical shapes, which also agrees with their SEM morphology (e.g., Fig. 5b) and a much severe sintering and coarsening due to the calcinations at 1300 °C.

UV–Vis diffuse reflectance spectrum

Figure 6 shows the UV–Vis diffuse reflectance spectra of $Zn_2Ti_xSn_{1-x}O_4$ ($x = 0, 0.1, 0.3, 0.5, 0.7, 0.9, 1.0$) prepared at 1100 °C for 2 h. The absorption edges of the $Zn_2Ti_xSn_{1-x}O_4$

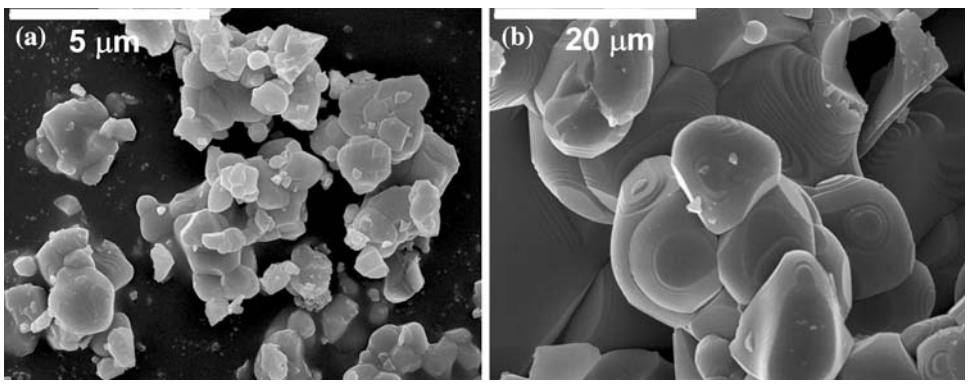

Fig. 5 SEM micrographs of $ZnTi_{0.5}Sn_{0.5}O_4$ prepared at **a** 1100 °C for 2 h and **b** 1300 °C for 2 h

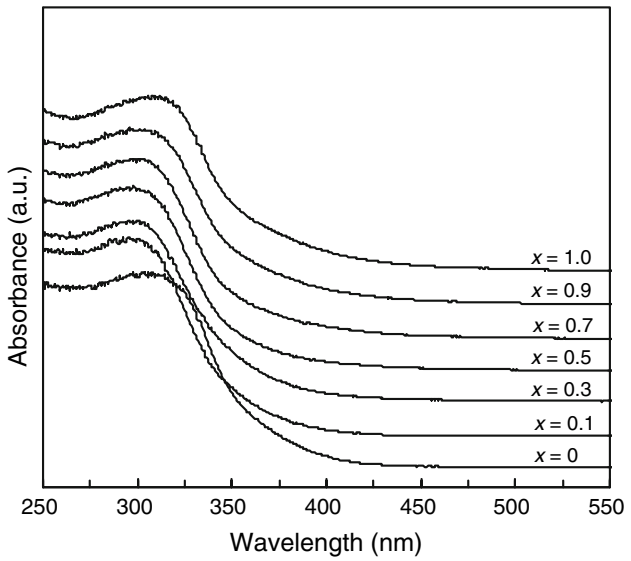

Fig. 6 UV–Vis diffuse reflectance spectra of $Zn_2Ti_xSn_{1-x}O_4$ ($x = 0$, 0.1, 0.3, 0.5, 0.7, 0.9, 1.0) prepared at 1100 °C for 2 h

samples, defined as the wavelengths at the intersections of the extrapolated horizontal and sharply rising portions of the UV–Vis absorption curves, were found near the ultraviolet region at 367, 357, 356, 353, 352, 359, and 362 nm for $x = 0$, 0.1, 0.3, 0.5, 0.7, 0.9, and 1.0, respectively. Thus, the adsorption edge decreased with increasing the Ti content up to $x = 0.7$ and then changed to increase for the Ti-rich samples ($x > 0.7$). These absorption edges were then used to obtain the band gap energies (E_g) of the $Zn_2Ti_xSn_{1-x}O_4$ ($x = 0$, 0.1, 0.3, 0.5, 0.7, 0.9, 1.0) samples [47] (Fig. 7), which indicate that the solid solution samples can be considered as mixed oxide semiconductors (E_g = 3.38–3.52 eV at $0 \leq x \leq 1.0$).

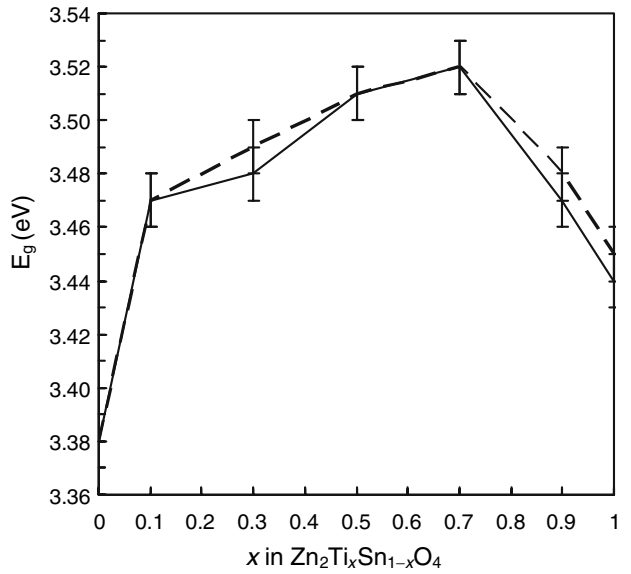

Fig. 7 Band gap energies (E_g) of $Zn_2Ti_xSn_{1-x}O_4$ ($x = 0$, 0.1, 0.3, 0.5, 0.7, 0.9, 1.0) powders prepared at 1100 °C for 2 h (*straight line*) and 1300 °C for 2 h (*dashed line*)

The dashed line in Fig. 7 shows the E_g data for the solid solutions prepared 1300 °C. It can be seen that the band gap energies (E_g) of the samples formed by calcination at 1300 °C were of little differences from those formed at 1100 °C. We also noted that the numbers of E_g also agree well with those of the samples produced from the solid-state reaction at 1300 °C [34]. Detailed discussion on the change of the optical absorptions with the sample composition (i.e., x) was given in our earlier paper [34].

Conclusions

A series of single-phase $Zn_2Ti_xSn_{1-x}O_4$ ($0 \leq x \leq 1$) solid solutions can be synthesized by calcination of the coprecipitated mixed $ZnO/TiO_2/SnO_2$ oxides at 1000 °C. The solid solutions thus prepared showed optical absorption in the near ultraviolet region. The composition or Ti content of $Zn_2Ti_xSn_{1-x}O_4$ had a significant effect on the absorption edge and thus the band gap energy of the solid solutions; the sample with $x = 0.7$ showed the biggest band gap energy (E_g = 3.52 eV). These tertiary oxide solid solutions are semiconductor materials that could be of potential for applications in optoelectronic, gas-sensing and microwave dielectric fields.

Acknowledgements The authors would like to thank Profs. Jianyuan Yu and Ruji Wang, and Mr. Jingzhi Wei for their help in this work. This work was financially supported by MOST of China (2003B86504).

References

1. Naidu HP, Virkar AV (1998) J Am Ceram Soc 81:2176
2. Edelman F, Hahn H, Seifried S, Alof C, Hoche H, Balogh A, Werner P, Zakrzewska K, Radecka M, Pasierb P, Chack A, Mikhelashvili V, Eisenstein G (2000) Mater Sci Eng B 69–70:386
3. Vinodgopal K, Bedja I, Kamat PV (1996) Chem Mater 8:2180
4. Oliveira MM, Schnitzler DC, Zarbin AJG (2003) Chem Mater 15:1903
5. Bedja I, Kamat PV (1995) J Phys Chem 99:9182
6. Taylor NW (1930) Z Physik Chem B 9:241
7. Dulin FH, Rase DE (1960) J Am Ceram Soc 43:125
8. Bartram SF, Slepetys RA (1961) J Am Ceram Soc 44:493
9. Yang J, Swisher JH (1996) Mater Charact 37:153
10. Marci G, Augugliaro V, Munoz MJL, Martin C, Palmisano L, Rives V, Schiavello M, Tilley RJD, Venezia AM (2001) J Phys Chem B 105:1033
11. Nikolic N, Sreckovic T, Ristic MM (2001) J Eur Ceram Soc 21:2071
12. Wang C, Wang XM, Zhao JC, Mai BX, Sheng GY, Peng PA, Fu JM (2002) J Mater Sci 37:2989. doi:10.1023/A:1016077216172
13. Wang C, Zhao JC, Wang XM, Mai BX, Sheng GY, Peng PA, Fu JM (2002) Appl Catal B Environ 39:269

14. Tennakone K, Kottegoda IRM, De Silva LAA, Perera VPS (1999) Semicond Sci Technol 14:975
15. Zakrzewska K (2001) Thin Solid Films 391:229
16. Kong LB, Ma J, Huang H (2002) J Alloys Compd 336:315
17. Lin J, Yu JC, Lo D, Lam SK (1999) J Catal 183:368
18. Radecka M, Zakrzewska K, Rekas M (1998) Sens Actuators B 47:194
19. Yamaguchi O, Morimi M, Kawabata H, Shimizu K (1987) J Am Ceram Soc 70:C-97
20. Chang YS, Chang YH, Chen IG, Chen GJ, Chai YL (2002) J Cryst Growth 243:319
21. Kim HT, Nahm S, Byun JD, Kim Y (1999) J Am Ceram Soc 82:3476
22. Kim HT, Byun JD, Kim Y (1998) Mater Res Bull 33:963
23. Chen ZX, Derking A, Koot W, Van Dijk MP (1996) J Catal 161:730
24. Hashemi T, Al-Allak HM, Illingsworth J, Brinkman AW, Woods J (1990) J Mater Sci Lett 9:776
25. Fang J, Huang AH, Zhu PX, Xu NS, Xie JQ, Chi JS, Feng SH, Xu RR, Wu MM (2001) Mater Res Bull 36:1391
26. Wu XH, Wang YD, Tian ZH, Liu HL, Zhou ZL, Li YF (2002) Solid-State Electron 46:715
27. Kovacheva D, Petrov K (1998) Solid State Ionics 109:327
28. Perkins JD, Del Cueto JA, Alleman JL, Warmsingh C, Keyes BM, Gedvilas LM, Parilla PA, To B, Readey DW, Ginley DS (2002) Thin Solid Films 411:152
29. Wu XH, Wang YD, Liu HL, Li YF, Zhou ZL (2002) Mater Lett 56:732
30. Yuan ZY, Huang F, Sun JT, Zhou YH (2002) Chem Lett 31:408
31. Coutts TJ, Young DL, Li X, Mulligan WP, Wu X (2000) J Vac Sci Technol A 18:2646
32. Belliard F, Connor PA, Irvine JTS (2000) Solid State Ionics 135:163
33. Yu JH, Choi GM (2001) Sens Actuators B 72:141
34. Wang C, Xu B-Q (2004) J Solid State Chem 177:3448
35. Wang C, Xu B-Q, Wang XM, Zhao JC (2005) J Solid State Chem 178:3500
36. Verwey EJW, Heilmann EL (1947) J Chem Phys 15:174
37. White WB, Deangelis BA (1967) Spectrochim Acta 23A:985
38. Ivanov VV, Talanov VM, Shabel'skaya NP (2001) Inorg Mater 37:839
39. Malavasi L, Galinetto P, Mozzati MC, Azzoni CB, Flor G (2002) Phys Chem Chem Phys 4:3876
40. Wang ZW, Downs RT, Pischedda V, Shetty R, Saxena SK, Zha CS, Zhao YS, Schiferl D, Waskowska A (2003) Phys Rev B 68:094101
41. Julien CM, Massot M (2003) Mater Sci Eng B 100:69
42. Julien CM, Massot M (2003) J Phys Condens Mater 15:3151
43. Keramidas VG, Deangelis BA, White WB (1975) J Solid State Chem 15:233
44. Wang ZW, Saxena SK, Zha CS (2002) Phys Rev B 66:024103
45. McCarty KF, Boehme DR (1989) J Solid State Chem 79:19
46. Chang RK, Lacina B, Pershan PS (1966) Phys Rev Lett 17:755
47. Hagfeldt A, Grätzel M (1995) Chem Rev 95:49